Molecular Biology of the Cell
Vol. 16, 3873–3886, August 2005

MLN64 Is Involved in Actin-mediated Dynamics of Late Endocytic Organelles[D] [V]

Maarit Hölttä-Vuori,*† Fabien Alpy,‡ Kimmo Tanhuanpää,† Eija Jokitalo,† Aino-Liisa Mutka,§ and Elina Ikonen*†

Institutes of *Biomedicine and †Biotechnology, University of Helsinki, 00014 Helsinki, Finland; ‡Département de Pathologie Moléculaire, Institut de Genetique et de Biologie Moleculaire et Cellulaire, 67404 Illkirch, Communauté Urbaine de Strasbourg, France; and §National Public Health Institute, 00300 Helsinki, Finland

Submitted December 22, 2004; Revised April 30, 2005; Accepted May 24, 2005
Monitoring Editor: Howard Riezman

MLN64 is a late endosomal cholesterol-binding membrane protein of an unknown function. Here, we show that MLN64 depletion results in the dispersion of late endocytic organelles to the cell periphery similarly as upon pharmacological actin disruption. The dispersed organelles in MLN64 knockdown cells exhibited decreased association with actin and the Arp2/3 complex subunit p34-Arc. MLN64 depletion was accompanied by impaired fusion of late endocytic organelles and delayed cargo degradation. MLN64 overexpression increased the number of actin and p34-Arc–positive patches on late endosomes, enhanced the fusion of late endocytic organelles in an actin-dependent manner, and stimulated the deposition of sterol in late endosomes harboring the protein. Overexpression of wild-type MLN64 was capable of rescuing the endosome dispersion in MLN64-depleted cells, whereas mutants of MLN64 defective in cholesterol binding were not, suggesting a functional connection between MLN64-mediated sterol transfer and actin-dependent late endosome dynamics. We propose that local sterol enrichment by MLN64 in the late endosomal membranes facilitates their association with actin, thereby governing actin-dependent fusion and degradative activity of late endocytic organelles.

INTRODUCTION

MLN64 is a late endosomal membrane protein with two functional domains: an N-terminal domain consisting of four transmembrane helices and a C-terminal steroidogenic acute regulatory protein (StAR)-related lipid transfer domain (START) that projects into the cytoplasm (Alpy *et al*., 2001, 2002). This topology suggested that MLN64 is a component of the machinery that facilitates cholesterol egress from late endosomes and lysosomes, possibly together with other proteins such as Niemann Pick Type C (NPC)1 and NPC2 (Alpy *et al*., 2001; Strauss *et al*., 2002). NPC1 or NPC2 mutations lead to late endosomal/lysosomal accumulation of cholesterol and other lipids, resulting in neurodegenerative disease (Ikonen and Hölttä-Vuori, 2004). Overexpression of MLN64 enhanced steroidogenesis (Watari *et al*., 1997), apparently by stimulating the mobilization of lysosomal cholesterol to the mitochondrial P450 cholesterol side chain cleavage enzyme, whereas mutant MLN64 lacking the START domain was reported to induce cholesterol accumulation in lysosomes (Zhang *et al*., 2002). These findings suggested that MLN64 plays a role in the maintenance of endosomal cholesterol flow and intracellular cholesterol homeostasis (Alpy *et al*., 2002; Zhang *et al*., 2002). Surprisingly, targeted mutation of the MLN64 START domain in mouse caused only modest alterations in cellular sterol metabolism and the mice were neurologically intact and fertile (Kishida *et al*., 2004), rather speaking against a crucial role for MLN64 in whole body cholesterol homeostasis.

In the present work, we studied the cellular phenotypes associated with MLN64 overexpression or depletion. We show that instead of decreasing late endosomal sterol levels, overexpression of MLN64 stimulated the accumulation of sterol in the organelles harboring the protein. Moreover, we provide evidence to suggest that MLN64-mediated sterol transfer operates in the actin-mediated dynamics of late endocytic organelles.

MATERIALS AND METHODS

Materials

C-terminal anti-MLN64 antibodies (2BE2F4) have been described previously (Moog-Lutz *et al*., 1997; Alpy *et al*., 2001). The mouse monoclonal N-terminal antibody (2D541) was raised against a synthetic peptide corresponding to residues 1–19 of human MLN64 protein (MSKLPRELTRDLERSLPAV). This peptide was coupled to ovalbumin (Sigma-Aldrich, St. Louis, MO) through an additional C-terminal cysteine. Generation of hybridomas was as described previously (Moog-Lutz *et al*., 1997). Anti-lysosome–associated membrane protein (Lamp) 1 (H4A3) and Lamp2 (H4B4) antibodies were from Developmental Studies Hybridoma Bank (University of Iowa, Iowa City, IA); anti-early endosomal autoantigen-1 (EEA1) antibodies were from BD Biosciences (San Jose, CA); anti-p34-Arc antibodies were from Upstate Biotechnology (Charlottesville, VA); and anti-β-tubulin, anti-actin, and anti-dynein IC antibodies (70.1) were from Sigma-Aldrich. Anti-lysobisphosphatidic acid (LBPA) antibodies were a generous gift from Jean Gruenberg (University of Geneva, Geneva, Switzerland), anti-Rab7 antibodies were from Marino Zerial (Max

This article was published online ahead of print in *MBC in Press* (http://www.molbiolcell.org/cgi/doi/10.1091/mbc.E04–12–1105) on June 1, 2005.

[D] [V] The online version of this article contains supplemental material at *MBC Online* (http://www.molbiolcell.org).

Address correspondence to: Elina Ikonen (elina.ikonen@helsinki.fi).

Abbreviations used: CytD, cytochalasin D; DHE, dehydroergosterol; DiI-LDL, 1,1′-dioctadecyl-3,3,3′,3′-tetramethyl-indocarbocyanine-perchlorate-labeled low density lipoprotein; EGF, epidermal growth factor; LBPA, lysobisphosphatidic acid; LDL, low-density lipoprotein; LPDS, lipoprotein-deficient serum; NPC, Niemann-Pick type C; PEG, polyethylene glycol; StAR, steroidogenic acute regulatory protein; START, StAR-related lipid transfer domain.

Planck Institute of Molecular Cell Biology and Genetics, Dresden, Germany), and anti-RILP antibodies were from Cecilia Bucci (University of Lecce, Lecce, Italy.) Cell culture media, filipin, dehydroergosterol (DHE), nocodazole, and cytochalasin D (CytD) were from Sigma-Aldrich. Alexa fluor 488- and 568-conjugated anti-IgG secondary antibodies, fluorescent endocytosed probes, and Alexa fluor 568-conjugated phalloidin were from Molecular Probes (Leiden, The Netherlands). FuGENE6 transfection reagent and polyethylene glycol (PEG) 1500 were from Roche Diagnostics (Mannheim, Germany). ECL Western blot detection reagents and radiolabeled lipids were from Amersham Biosciences (Freiburg, Germany).

cDNA Constructs and Short Interfering RNA (siRNA) Oligonucleotides

Wild-type (WT) MLN64 and ΔSTART in pSG5 vectors were as described previously (Alpy *et al*., 2001). The pSG5 MLN64 M307R, N311D mutant was generated by site-directed mutagenesis with QuikChange site-directed mutagenesis kit (Stratagene, La Jolla, CA) and synthetic oligonucleotide 5′-GCCCGAGAGG AGAGTACTGT GGGACAAGAC AGTGAC. N-terminal green fluorescent protein (GFP) fusion constructs were obtained by subcloning the cDNAs in pEGFP-N vectors (BD Biosciences Clontech, Palo Alto, CA). The HA-RILP construct was a kind gift from Cecilia Bucci (University of Lecce, Lecce, Italy). For siRNA, oligonucleotide duplex was designed against the target sequence 5′-AACACAGGCATCCGTAAGAAC of MLN64. The control RNA (GL2) against firefly luciferase has been described previously (Elbashir *et al*., 2001). For experiments, both nontagged and sense strand 5′-biotin-labeled oligos were used (Proligo, Hamburg, Germany). The transfection frequency of siRNAs was assessed by fluorescence microscopy detection of biotin-tagged oligos with fluorescently labeled streptavidin (Jackson ImmunoResearch Laboratories, West Grove, PA) and was typically ≥90%. No difference in the MLN64 depletion efficiency was observed between tagged and nontagged oligos.

Cell Culture and Transfection

COS-1 and HeLa cells were cultured in DMEM containing 10% fetal bovine serum, 100 U/ml penicillin, and 100 μg/ml streptomycin. NPC1 93.41 fibroblasts were cultured as described previously (Hölttä-Vuori *et al*., 2000). For siRNA transfections in HeLa cells, either Oligofectamine or Lipofectamine 2000 transfection reagents (Invitrogen, Carlsbad, CA) was used. The siRNA transfections and plasmid cotransfections were performed as described previously (Elbashir *et al*., 2001). Cells were replated and retransfected 2–3 d after the first transfection and used for experiments at 5–6 d of transfection. To overcome the siRNA-mediated gene silencing by plasmid overexpression (Elbashir *et al*., 2001), plasmids encoding MLN64 or its mutants were included in the first round of transfection to achieve detectable expression level. For HA-RILP, the plasmid was cotransfected for the last 2 d. COS-1 cells were transfected with FuGENE6 and NPC 93.41 fibroblasts by electroporation. Electroporation was carried out in 400 μl of Eagle's minimum essential medium containing 20 mM PIPES, pH 7.0, 128 mM glutamate, 10 μM Ca-acetate, 2 mM Mg-acetate using 800-μF capacitance and 400 V.

Immunocytochemistry and Microscopy

Immunocytochemistry was performed essentially as described previously (Hölttä-Vuori *et al*., 2002). The cytoskeleton-preserving fixation (cytoskeletal fix) was 2.6% paraformaldehyde in 2-(*N*-morpholino)ethanesulfonic acid buffer with 160 mM HEPES and 320 mM sucrose. To label actin, cells were fixed with cytoskeletal fix and permeabilized with 500 μg/ml filipin supplemented with Alexa 568-labeled phalloidin. For anti-p34-Arc stainings, the cells were fixed with −20°C methanol for 2 min. The coverslips were viewed with TCS SP or TCS SP2 confocal microscopes (Leica, Wetzlar, Germany), Zeiss Axiophot photomicroscope or IX70 inverted microscope (Olympus, Tokyo, Japan) equipped with a Polychrome IV monochromator (TILL Photonics, Gräfelfing, Germany) with appropriate filters. For live cell microscopy, the images were obtained with TILL Photonics system and processed with TILL Vision 4 and Image ProPlus 4.5 software. For three-dimensional projections, image stacks were deconvoluted with adaptive three-dimensional (3D) deconvolution in Autoquant Autodeblur, and the 3D reconstructions were made with Bitplane Imaris.

Interaction of Recombinant MLN64-START Domain and Photocholesterol

The construct encoding the N-terminal His-tagged human MLN64 START domain (residues 216–444) cloned into the pET22b vector (Tsujishita and Hurley, 2000) was a kind gift from Yosuke Tsujishita and James H. Hurley (National Institutes of Health, Bethesda, MD). WT and mutant His-tagged MLN64 START domains were expressed in *Escherichia coli* BL21 (DE3) (Stratagene, La Jolla, CA) and purified using Ni-NTA affinity resin (QIAGEN, Valencia, CA). The purified proteins were then dialyzed against 150 mM NaCl and 20 mM Tris-HCl. [^{3}H]Photocholesterol (Thiele *et al*., 2000) was a kind gift from Christoph Thiele (Max Planck Institute of Molecular Cell Biology and Genetics, Dresden, Germany). The purified His-tagged WT and mutant MLN64 START domains were incubated with 10 μCi of [^{3}H]photocholesterol in 150 mM NaCl, 50 mM Tris-HCl, pH 7.4, 2% (vol/vol) ethanol for 15 min at 37°C and irradiated for 10 min at 4°C under UV light using filtered (340 ± 40 nm) beam of a high-pressure 50-W mercury lamp. Irradiated proteins were analyzed by SDS–PAGE and fluorography.

Labeling with Fluorescent Endocytosed Probes

For 1,1′-dioctadecyl-3,3,3′,3′-tetramethyl-indocarbocyanine-perchlorate-labeled low-density lipoprotein (DiI-LDL) labeling, cells were incubated with 10 μg/ml DiI-LDL for 15–30 min in serum-free culture medium, washed and further incubated in serum-free medium for >1.5 h to allow DiI-LDL to reach late endocytic compartments. Cells were then fixed or used for live cell microscopy. For epidermal growth factor (EGF) labeling, the cells were incubated with 500 ng/ml rhodamine-epidermal growth factor in serum-free culture medium with 1% bovine serum albumin, washed, further incubated in the same medium for indicated times, and then fixed. For subsequent antibody staining, the cells were permeabilized with 0.1% Triton X-100. The analysis of EGF degradation was performed as described previously (Raiborg *et al*., 2001), and the mean fluorescence intensity of cells was analyzed with Image ProPlus 4.5 software. For labeling with fluorescent dextrans, the cells were incubated with 1 mg/ml dextran overnight in serum-free culture medium, washed, and further incubated in normal growth medium for >2 h to allow the probe to reach late endocytic compartments.

Labeling with Dehydroergosterol (DHE)

DHE-methyl-β-cyclodextrin complexes were prepared as described previously (Hao *et al*., 2002). Final concentration of DHE used for labeling cells was 1 mM. The cells were labeled for 1 min, further incubated as indicated, and monitored live with TILL Photonics system equipped with appropriate filters (Mukherjee *et al*., 1998). The total fluorescence intensities of both GFP and DHE signals from single endosomes were analyzed with Image ProPlus 4.5 software. Nonspecific background was subtracted from DHE images before intensity measurements.

Electron Microscopy

For immunoelectron microscopy, cells were fixed with PLP fixative (2% formaldehyde, 0.01 M periodate, and 0.075 M lysine-HCl in 0.075 M phosphate buffer, pH 7.4) for 2 h at room temperature. Cells were permeabilized with 0.01% saponin (Sigma-Aldrich) and immunolabeled by using anti-MLN64 C-terminal antibodies and 1.4-nm gold particle-conjugated Fab′-fragments against mouse IgM + IgG (Nanoprobes, Yaphank, NY). Nanogold was silver enhanced with an HQ silver kit (Nanoprobes) for 0.5–4 min and gold toned with 0.05% gold chloride (Arai *et al*., 1992). Cells were then processed for Epon embedding as described previously (Seemann *et al*., 2000). Sections were cut parallel to the coverslip, picked up on single-slot copper grids, poststained with uranyl acetate and lead citrate, and examined with a FEI Tecnai 12 transmission electron microscope at 80 kV.

Cell Fusions

The protocol was modified from Zhang *et al*. (2001). Briefly, cells labeled with fluorescent dextrans and/or transfected with WT MLN64-GFP or ΔSTART-GFP were cocultured overnight and incubated with 50% PEG 1500 for 5 min at room temperature. After fusion the cells were washed and incubated in the normal growth medium for 1 h and fixed with cytoskeletal fix. Colocalization of the signals was analyzed with Image ProPlus 4.5 software using Pearson's correlation (Blom *et al*., 2003). Nonspecific background was subtracted from images before colocalization analysis.

Cell Fractionation and Western Blotting

To analyze the membrane association of proteins, the cells were harvested and the postnuclear supernatant (PNS) was prepared in phosphate-buffered saline (PBS) supplemented with protease inhibitors (chymostatin, leupeptin, antipain, and pepstatin, at 25 μg/ml each). The PNS was centrifuged at 100,000 × *g* for 1 h. The supernatants were collected, and the membranes harvested in 1% Nonidet P-40 in PBS. Western blot analysis was performed as described previously (Hölttä-Vuori *et al*., 2002). To analyze actin-dependent sedimentation of late endocytic organelles, a protocol modified from Richardson *et al*. (2004) was used. Briefly, PNS was prepared as described above, and 30-μg aliquots of PNS protein was incubated in the presence of 1 mM magnesium acetate and 100 μM nocodazole, with or without 4 μM cytochalasin D for 30 min at 37°C. Pellets obtained after centrifugation at 100,000 × *g* for 5 min as well as samples of total input protein before centrifugation (30 μg) were immunoblotted with the indicated antibodies.

Cholesterol Biochemistry

Cholesterol esterification in lipoprotein-starved cells was measured as incorporation of [^{3}H]oleic acid into cholesteryl esters as described previously (Hölttä-Vuori *et al*., 2002). To analyze esterification in the presence of low-density lipoprotein (LDL), cells were otherwise processed identically to lipoprotein-starved cells, but the labeling medium was supplemented with 50 μg/ml LDL. For cholesterol efflux measurement, cells were labeled for 1–

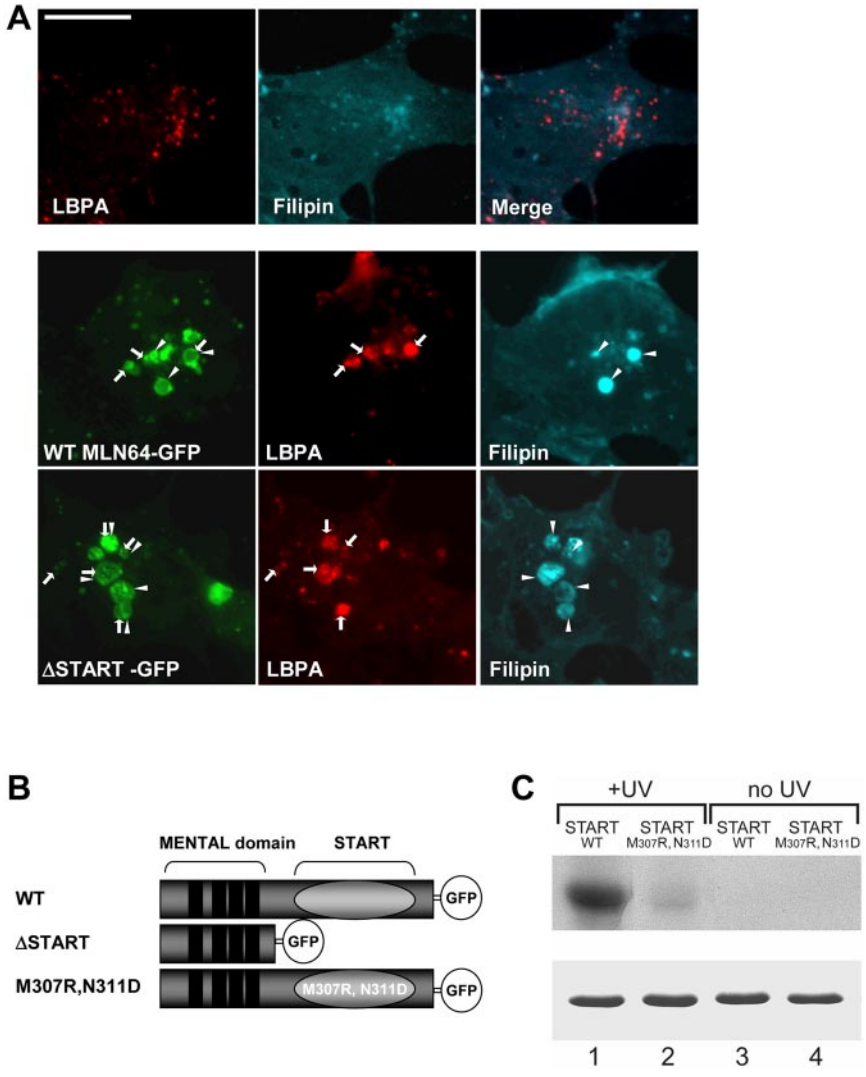

Figure 1. MLN64 overexpression in COS cells. (A) Nontransfected cells or cells overexpressing GFP-fused WT MLN64 or ΔSTART were stained with filipin and anti-LBPA antibodies. Arrows, MLN64-positive organelles containing LBPA. Arrowheads, MLN64-positive organelles containing filipin. Bar, 10 μm. (B) Schematic representation of WT and mutant MLN64 cDNAs used. (C) WT (lanes 1 and 3) and M307R, N311D mutant (lanes 2 and 4) MLN64 START domains were incubated with [^{3}H]photocholesterol and either UV-irradiated or not. After SDS-PAGE, cross-linked [^{3}H]cholesterol was revealed by fluorography (top). For comparison, similar amounts of recombinant proteins were stained with Coomassie Blue after SDS-PAGE (bottom).

2 d with [^{3}H]cholesterol in lipoprotein-deficient medium, washed thoroughly, and incubated with 5 mM methyl-β-cyclodextrin for 5 min at 37°C. The media and cells were collected, and the percentage of cholesterol effluxed was calculated as percentage of radioactivity in medium versus total (cells + medium).

Statistical Analysis

Statistical significance was analyzed by student's two-tailed *t* test. Error bars in figures represent SEM.

RESULTS

Overexpression of MLN64 Stimulates Sterol Deposition in Late Endocytic Organelles

In COS-1 cells, both WT MLN64 and a mutant lacking the sterol-binding domain (ΔSTART) localized to late endosomes as described previously (Zhang *et al*., 2002) (Figure 1A). The late endosomal compartments are considered to be enriched in LBPA but relatively cholesterol poor (Kobayashi *et al*., 2002; Möbius *et al*., 2003) (Figure 1A). We found that both WT and ΔSTART MLN64 induced the accumulation of cholesterol and/or LBPA in enlarged late endocytic organelles as assessed by filipin fluorescence and antibody staining, respectively (Figure 1A). However, the amount of deposited lipid varied between individual endosomes. The overexpression of ΔSTART typically created grossly enlarged endosomes with loosely packed internal structures, whereas with the WT protein, the endosome enlargement was less conspicuous and the organelles more compact (Figure 1A).

To clarify the role of cholesterol binding in MLN64 function, we generated a mutant protein compromised in cholesterol binding. The START domain protein family can be divided into different groups according to their lipid binding specificities. For example, StAR and MLN64 are cholesterol binding proteins (Tsujishita and Hurley, 2000), whereas phosphatidylcholine transfer protein (PCTP) directly binds phosphatidylcholine (Westerman *et al*., 1983). The lipid binding specificity of START domains is most probably determined by specific residues in the tunnel wall formed by the three-dimensional folding of the START domain (Tsujishita and Hurley, 2000). Multi-alignment of these regions revealed the presence of two uncharged residues in MLN64, Met 307 and Asn 311, that are conserved in the cholesterol-binding START domain of StAR but replaced by two charged residues in the START domain of PCTP. Based on this structural divergence, we created a mutant MLN64 START domain construct where Met 307 and Asn 311 were changed into Arg 307 and Asp 311, respectively (Figure 1B).

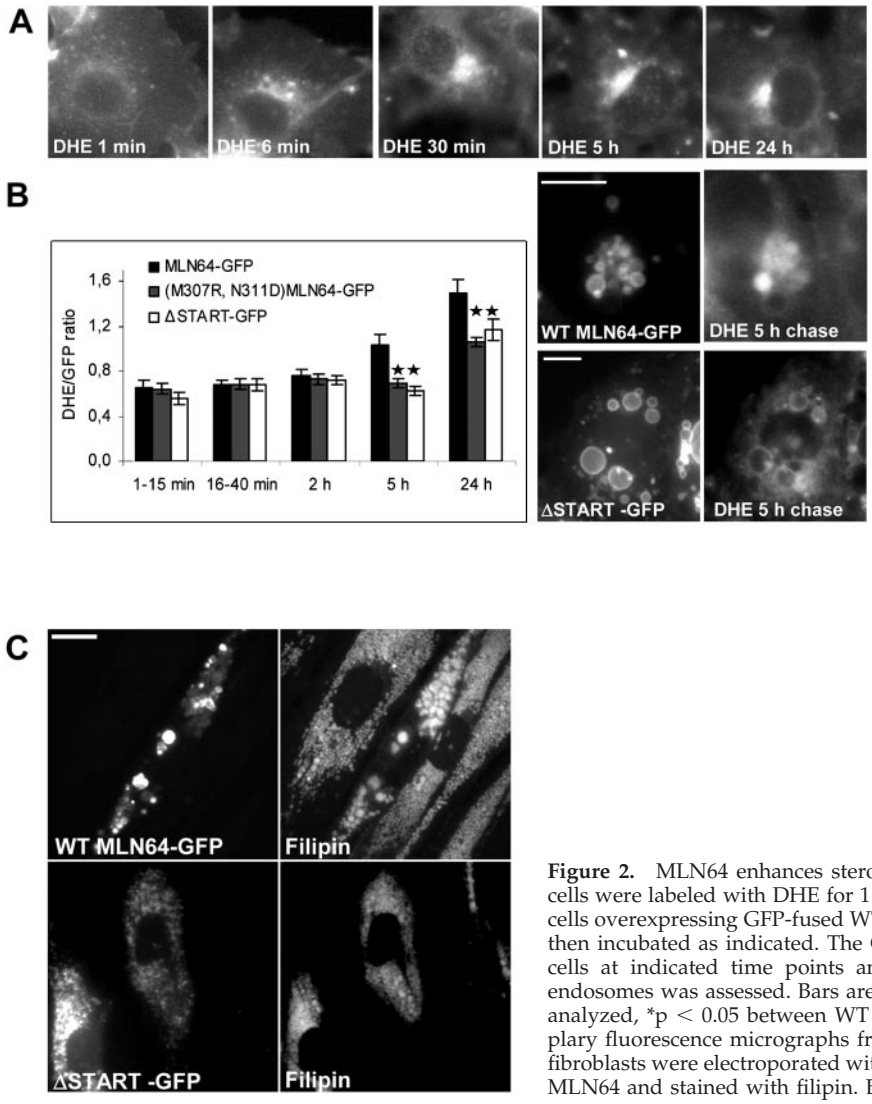

Figure 2. MLN64 enhances sterol deposition within late endosomes. (A) COS-1 cells were labeled with DHE for 1 min and then incubated as indicated. (B) COS-1 cells overexpressing GFP-fused WT or mutant MLN64 were labeled with DHE and then incubated as indicated. The GFP and DHE signals were imaged from living cells at indicated time points and the intensity ratio of DHE versus GFP in endosomes was assessed. Bars are mean intensity ratios from 18 to 54 endosomes analyzed, *$p < 0.05$ between WT MLN64 and M307R,N311D or ΔSTART. Exemplary fluorescence micrographs from 5-h chase are shown. Bars, 10 μm. (C) NPC fibroblasts were electroporated with plasmids encoding GFP-fused WT or ΔSTART MLN64 and stained with filipin. Bars, 20 μm.

The cholesterol binding properties of both WT and M307R, N311D START domains of MLN64 were further studied in vitro. Purified recombinant WT and M307R, N311D START domains were incubated with the photo-activatable cholesterol analogue [^{3}H]photocholesterol (Thiele *et al*., 2000). Covalent binding of cholesterol was achieved by UV irradiation, and complexes were analyzed by SDS-PAGE and fluorography (Figure 1C). We found that WT MLN64 START domain bound cholesterol efficiently, whereas the M307R, N311D mutant MLN64 START domain did not (Figure 1C). These results indicate that the two residues Met 307 and Asn 311 present within the MLN64 START domain are critical for cholesterol binding. The same mutation was then introduced into an MLN64 expression vector to generate a mutant MLN64 protein defective in cholesterol binding.

To follow MLN64-mediated sterol transfer in vivo, we labeled COS cells transfected with GFP-fused WT, ΔSTART or M307R, N311D MLN64 with the fluorescent cholesterol analogue DHE for 1 min and followed its distribution. In nontransfected cells, DHE initially labeled the plasma membrane and was rapidly internalized, also visualizing the juxtanuclear region that encompassed Rab11-positive recycling endosomes (Figure 2A; our unpublished data). This labeling pattern persisted for at least 24 h and is in accor-

Figure 3 (facing page). Characterization of MLN64 overexpression and knockdown in HeLa cells. (A) Cells overexpressing WT MLN64-GFP were stained with anti-Lamp1 antibodies. Images are confocal and represent a single focal plane. Bar, 20 μm. (B) WT MLN64-transfected cells were processed for immunoelectron microscopy with anti-MLN64 C-terminal antibodies. Bar, 200 nm. (C) Cells were transfected with control siRNA oligos (GL2) or oligos targeted against MLN64 (MLN64siRNA). Cell lysates (30 μg of protein) were analyzed by Western blotting using anti-MLN64 C-terminal antibodies. The amount of MLN64 protein was determined by densitometric scanning and expressed as a percentage of the protein in MLN64-depleted versus control cells (mean from 4 experiments). (D) Control RNA transfected (GL2) or MLN64-depleted cells (MLN64siRNA) were labeled with DiI-LDL, fixed, and stained with filipin and Lamp1-antibodies. Bars, 20 μm. (E) Quantification of the dispersal of DiI-LDL–positive organelles. Cells were transfected with siRNAs alone or cotransfected with plasmids encoding GFP-fused WT or mutant MLN64 cDNAs. The cells were then labeled with DiI-LDL before fixation. The bars represent percentage of cells with perinuclear clustering of DiI-LDL–positive organelles (2–10 independent experiments, n = 48–605 cells).

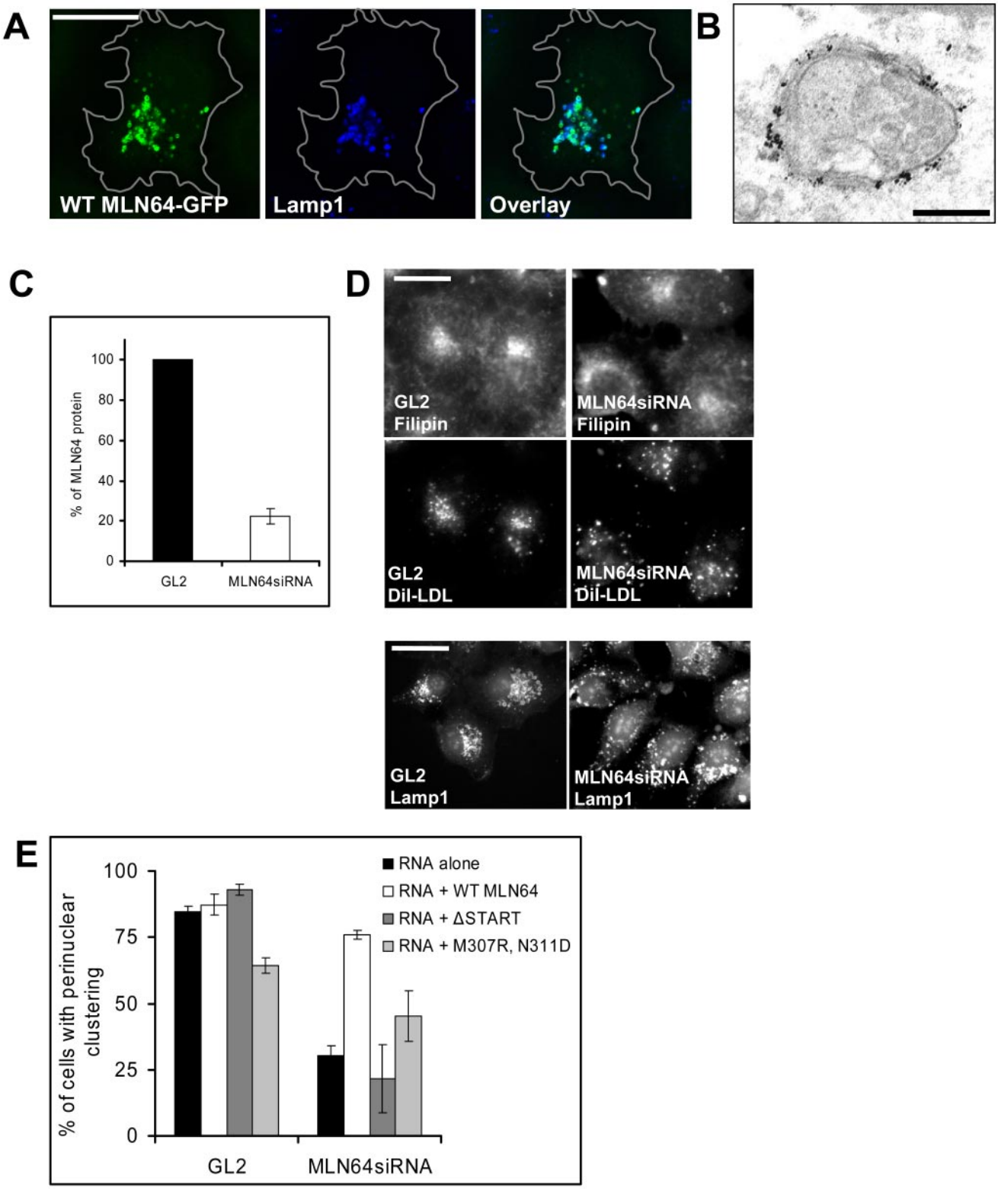
A
WT MLN64-GFP
Lamp1
Overlay
B
C
% of MLN64 protein
100
80
60
40
20
0
GL2
MLN64siRNA
D
GL2
Filipin
MLN64siRNA
Filipin
GL2
DiI-LDL
MLN64siRNA
DiI-LDL
GL2
Lamp1
MLN64siRNA
Lamp1
E
% of cells with perinuclear clustering
100
75
50
25
0
GL2
MLN64siRNA
RNA alone
RNA + WT MLN64
RNA + ΔSTART
RNA + M307R, N311D

Figure 3.

dance with that observed in Chinese hamster ovary cells (Mukherjee *et al*., 1998). In MLN64-transfected cells, some DHE reached MLN64-positive endosomes already at early time points (under 15 min of chase). With all the constructs, the DHE intensity in the endosomes was proportional to the GFP fluorescence intensity. To compare the degree of endosomal DHE deposition between constructs, the intensity ratio DHE/GFP was calculated. In WT MLN64-containing endosomes, the relative intensity of DHE increased upon chasing, being evident at 5 and 24 h of chase (Figure 2B). In the organelles expressing ΔSTART or M307R, N311D mutant proteins, the increase in DHE was more moderate and the DHE/GFP ratio significantly lower than in WT MLN64-expressing endosomes (Figure 2B).

To assess the effect of MLN64 on cholesterol-laden membranes, we overexpressed WT and ΔSTART MLN64 in NPC1-deficient 93.41 fibroblasts harboring massive late endosomal cholesterol accumulation (Figure 2C). It has been shown that MLN64 overexpression does not complement the cholesterol accumulation in NPC2-deficient fibroblasts (Alpy *et al*., 2001). Analogously, the cholesterol deposits were not cleared in NPC1 fibroblasts upon MLN64 overexpression (Figure 2C). Instead, overexpression of WT MLN64 often created bigger cholesterol-filled structures harboring the protein. This effect was not observed upon ΔSTART overexpression (Figure 2C).

Depletion of MLN64 Results in the Scattering of Late Endocytic Cargo Bearing Organelles and Inhibits Endosomal Degradation

In HeLa cells, MLN64 localized to late endocytic organelles as observed by good colocalization with lysosome-associated Lamp1 but not with early endosomal EEA1 (Figure 3A; our unpublished data). In comparison with COS cells, MLN64 overexpression was not accompanied by a striking increase in the endosome size. By immunoelectron microscopy, the distribution of MLN64 in the limiting late endosomal membrane was uneven (Figure 3B). This agrees with previous observations of MLN64 localization in MCF7 cells overexpressing MLN64 (Alpy *et al*., 2001).

The depletion of MLN64 in HeLa cells was achieved by siRNA transfection. A 70–90% reduction in the protein level was obtained in 5–6 d (Figure 3C). Depletion of MLN64 did not grossly affect cellular cholesterol distribution as assessed by filipin staining: in particular, an NPC-like endosomal cholesterol accumulation was not observed (Figure 3D). Furthermore, no impeding effect of MLN64 depletion on cholesterol homeostasis was found in biochemical measurements. Cholesterol esterification was normal both in cells cultured in lipoprotein-deficient medium and upon LDL feeding (109.1 ± 8.9 and 107.6 ± 7.5% of control, respectively; SEM, n = 6 in both experiments). The efflux of radiolabeled cholesterol to methyl-β-cyclodextrin was moderately enhanced upon MLN64 depletion (31.7 ± 1.0% effluxed from control cells and 41.4 ± 1.7% from MLN64-depleted cells; SEM, n = 6 in both experiments). These results are in accordance with recent work demonstrating that targeted mutation of MLN64 START had no profound effects on sterol metabolism (Kishida *et al*., 2004).

However, we observed a marked difference in the localization of internalized DiI-labeled LDL upon MLN64 depletion (Figure 3D). When the cells were incubated with DiI-LDL for 30 min and chased for 1.5–2 h, DiI-LDL accumulated in the perinuclear cluster of late endosomes/lysosomes in control cells, whereas in MLN64-depleted cells the DiI-LDL–labeled organelles were redistributed to the cell periphery. The dispersed organelles were late endocytic organelles because DiI-LDL largely colocalized with Lamp1 staining in MLN64-depleted cells (our unpublished data). Moreover, the distribution of Lamp1 itself was affected similarly to DiI-LDL, as shown by partial scattering of Lamp1 antibody labeling to the cell periphery (Figures 3D and 4A). The perinuclear localization of DiI-LDL–labeled endosomes was found in 85% of control cells but in only 30% of MLN64-depleted cells (Figure 3E). When the cells were cotransfected with a plasmid encoding WT MLN64, the perinuclear accumulation of DiI-LDL–containing organelles was restored in MLN64 depleted cells, indicating that the phenomenon was specifically due to the lack of MLN64 protein (Figure 3E). Moreover, both the ΔSTART and M307R,N311D mutant proteins were unable to rescue the late endosome dispersion.

Other receptor-mediated cargo destined for degradation, such as EGF, also was retained in the peripheral endosomes in MLN64-depleted cells (Figure 4A). In addition, we found that the degradation of rhodamine-epidermal growth factor was retarded in MLN64 depleted cells compared with control (Figure 4B). Moreover, the hydrolysis of LDL-derived cholesteryl esters was slightly inhibited in MLN64-depleted cells (our unpublished data). The retardation in degradation was apparently not due to defective sorting from early to late endosomes: after 30 min of rhodamine-epidermal growth factor labeling followed by additional 1.5-h incubation, EGF was cleared from organelles containing EEA1 and found mostly in Lamp1-positive organelles (Figure 4A). It is possible that the subpopulation of dispersed late endocytic organelles represents a compartment preceding terminal hydrolytic lysosomes and that the confinement of cargo in this compartment retards its degradation. The dispersion phenotype was not limited to receptor-mediated cargo, because fluorescently labeled dextrans were redistributed to the peripheral late endosomes upon MLN64 depletion similarly to DiI-LDL and EGF (our unpublished data).

A similar effect (dispersal of late endocytic organelles and impaired cargo degradation) has been reported upon expression of dominant-negative mutants of Rab7 (Vitelli *et al*., 1997). This is due to impaired recruitment of the microtubule-associated dynein motors on late endosomes by the Rab7 effector RILP (Cantalupo *et al*., 2001; Jordens *et al*., 2001). Because the membrane association of Rab7 was shown to depend on the cholesterol content of the endosomal membranes (Lebrand *et al*., 2002), we hypothesized that the function of MLN64 may be related to the recruitment of this machinery. To test this, we analyzed the expression levels and membrane association of Rab7 and dynein in control and MLN64-depleted cells. The levels of dynein and Rab7 were not significantly altered upon MLN64 depletion (Figure 5A), and the proteins were predominantly membrane associated (Figure 5B). Both in control and MLN64 siRNA-treated cells, overexpression of RILP resulted in the juxtanuclear clustering of enlarged endosomes harboring the protein (Figure 5C). However, RILP overexpression was unable to rescue the scattering of DiI-LDL–labeled endosomes in the majority of MLN64-depleted cells (Figure 5C). Together, these data suggest that MLN64 depletion did not impair the late endosomal recruitment of the Rab7–RILP–dynein machinery.

MLN64 Modulates the Association of Actin with Late Endosomes and Affects Actin-dependent Fusion of Late Endocytic Organelles

To analyze how MLN64 influences late endosome movement, we followed the trafficking of DiI-LDL–labeled endosomes in control and MLN64-depleted cells. In control cells,

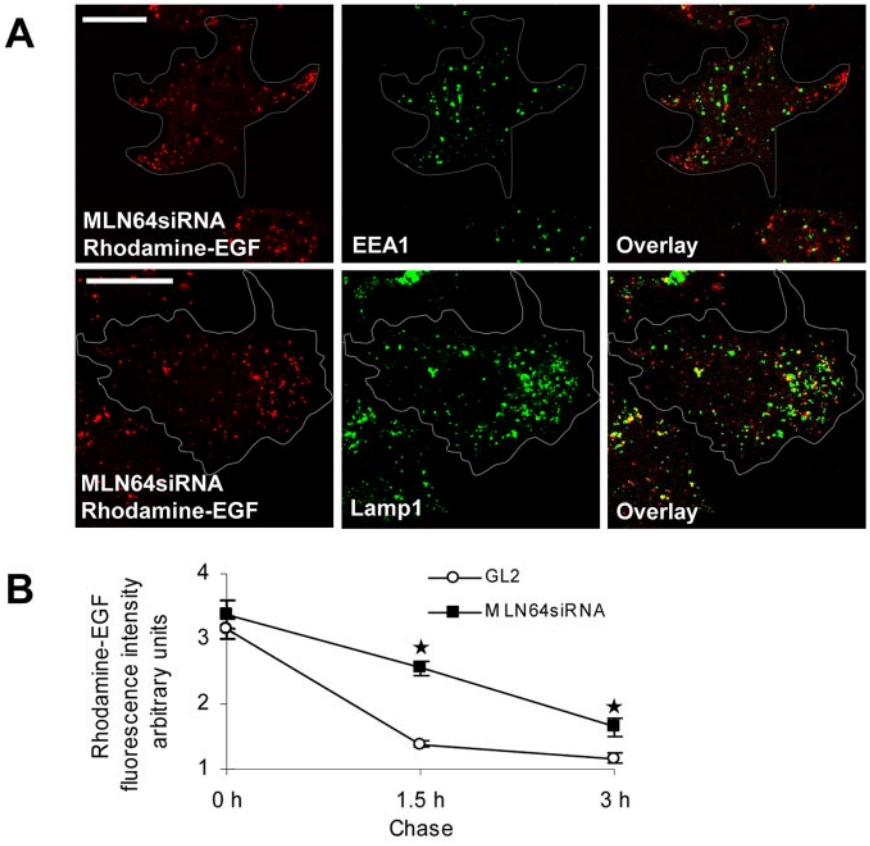

Figure 4. Depletion of MLN64 does not impair the sorting of EGF from early endosomes but retards EGF degradation. (A) MLN64-depleted cells (MLN64siRNA) were incubated with rhodamine-labeled EGF for 30 min, further incubated for 1.5 h, fixed, and stained with antibodies against EEA1 and Lamp1. Images are confocal and represent a single focal plane. Bars, 20 μm. (B) Control (GL2) or MLN64-depleted cells (MLN64siRNA) were fed rhodamine-labeled EGF for 1 h and further incubated for 1.5 or 3 h. The mean intensity of cell-associated EGF fluorescence was analyzed from 15 cells at each time point, *$p < 0.05$ between GL2 control and MLN64siRNA.

the endosomes exhibited bidirectional movements to and from the cell periphery (Figure 6, A and C, and Supplemental Videos 1 and 3) at an average velocity of ~0.6 μm/s. This movement was microtubule dependent because it was inhibited by the microtubule-depolymerizing agent nocodazole (Supplemental Figure 1). In MLN64-depleted cells, the DiI-LDL–labeled endosomes typically traveled in the cell periphery producing trajectories that often outlined the cell (Figure 6B and Supplemental Video 2). Such an altered pattern of endosome movement was observed in ~80% of MLN64 knockdown cells. The average velocity of these organelles was comparable with that in control cells. The movement also was dependent on microtubules as judged by the loss of organelle motility upon nocodazole treatment (Supplemental Figure 1). Pharmacological disruption of actin has been shown to alter the movement of late endosomes, resulting in lost bidirectionality, rapid random movements, and dispersion of cargo-containing organelles to the cell periphery (Durrbach *et al.*, 1996; Cordonnier *et al.*, 2001). Indeed, when control HeLa cells were incubated with 0.2 μM cytochalasin D, the DiI-LDL–labeled endosomes exhibited movements that were closely similar to those observed upon MLN64 depletion (Figure 6D and Supplemental Video 4). The bidirectional, stellate trajectories were lost and the tracks typically outlined the cell periphery.

It has been shown that the fusion of late endosomes with preexisting lysosomes (van Deurs *et al.*, 1995) and with each other (Kjeken *et al.*, 2004) is facilitated by actin in mammalian cells. In addition, homotypic fusion of vacuoles in yeast has been shown to be regulated by organelle-bound actin (Eitzen *et al.*, 2002). The enlargement of late endosomes upon MLN64 overexpression (Figures 1A and 2, B and C) suggested a potential role for the protein in the fusion of late endocytic organelles. To assess endosome fusion, we analyzed the ability of late endosomes and/or lysosomes to mix in control or MLN64-depleted HeLa cells fused with PEG. The cells were incubated with either rhodamine- or fluorescein-labeled dextran overnight, cocultured, fused with PEG, and further incubated for 1 h. The degree of mixing of the green and red signals was assessed as a measure of endosome clustering and/or fusion. At this time point, significant overlap of the signals was found in control cells (Figure 7). When cells were incubated with 0.2 μM cytochalasin D, the signal overlap was greatly reduced. This argues for the involvement of the actin cytoskeleton in the process that leads to the fusion of late endocytic organelles. The low cytochalasin D concentration applied did not grossly affect cell morphology (Figure 7). Analogously to the actin perturbation, the depletion of MLN64 significantly inhibited endosome fusion as suggested by the reduced signal overlap (Figure 7). To analyze the effect of MLN64 overexpression, WT MLN64-GFP or ΔSTART-GFP–expressing cells were fused with rhodamine dextran–labeled cells and endosome fusion monitored similarly as described above. We found WT MLN64 overexpression to stimulate the fusion of late endocytic organelles approximately two- to threefold, whereas ΔSTART had no significant effect (Figure 7). The enhancement was cytochalasin D sensitive, suggesting that MLN64 is involved in the actin-mediated fusion of late endocytic organelles. It is possible that MLN64 has direct fusogenic activity, but the effects on endosome fusion also could be secondary to the effects on endosome positioning: peripherally scattered endosomes could simply have fewer opportunities to engage in fusion compared with perinuclearly clustered endosomes.

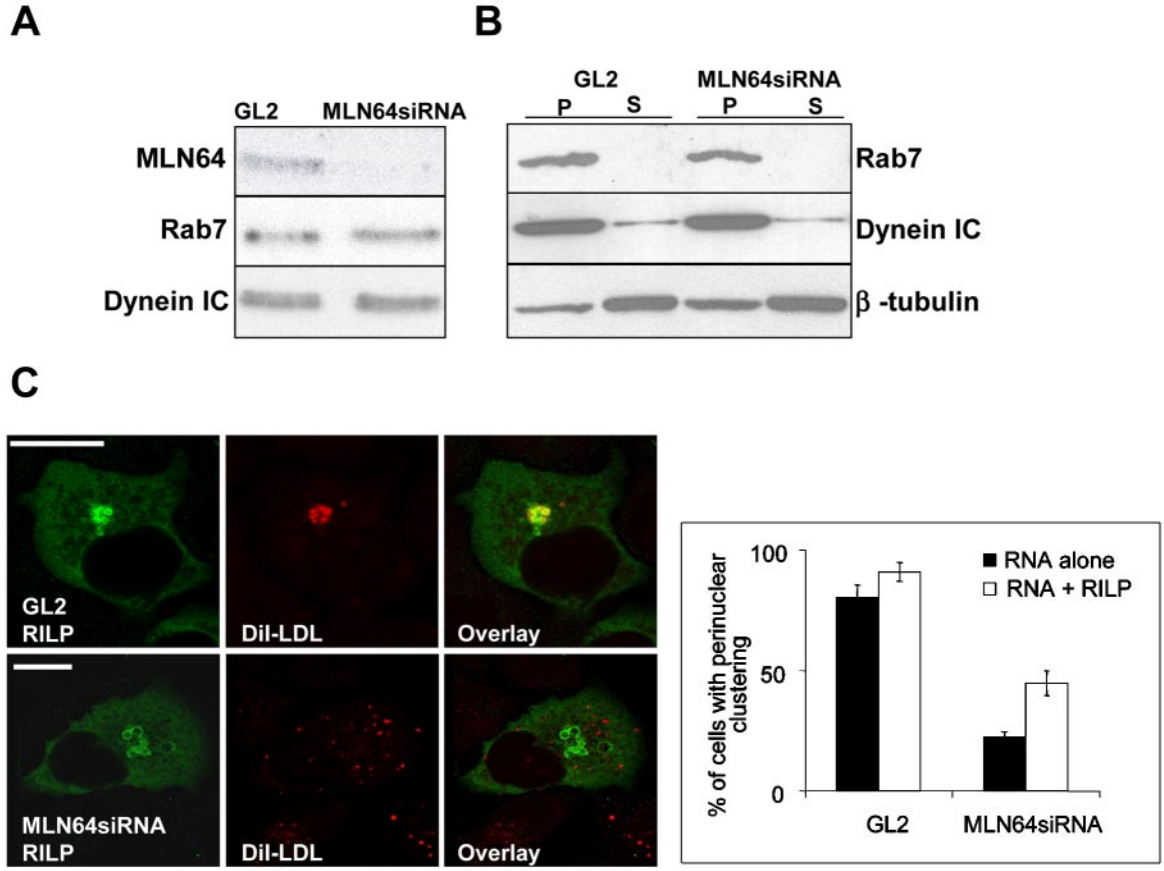

Figure 5. Rab7-RILP-dynein machinery in MLN64-depleted HeLa cells. (A) Cells were transfected with control siRNA oligos (GL2) or oligos targeted against MLN64 (MLN64siRNA). Aliquots (30 μg) of cell lysates were analyzed by Western blotting using anti-MLN64 C-terminal, anti-Rab, or anti-dynein IC antibodies. (B) PNS from control (GL2) or MLN64-depleted cells (MLN64siRNA) was pelleted at 100 000 g and total membrane pellets (P) and supernatants (S) analyzed by Western blotting using anti-Rab7, anti-dynein IC, or anti-β-tubulin antibodies. (C) Cells were transfected with siRNAs alone or cotransfected with a plasmid encoding HA-tagged RILP, labeled with DiI-LDL, fixed and stained with anti-RILP antibodies. Bars represent percentage of cells with perinuclear clustering of DiI-LDL–positive organelles from two independent experiments (111–158 cells in total). Images are confocal and represent a single focal plane. Bars, 20 μm.

These observations led us to study actin organization in HeLa cells overexpressing or depleted of MLN64. The overall organization of the actin cytoskeleton was not perturbed upon altering the level of MLN64 protein (our unpublished data). In control cells, a subset (~20%) of dextran-labeled late endocytic organelles was decorated with actin patches or extensions (Figure 8A). This is in accordance with a recent study demonstrating that a subset of late endosomes can nucleate actin in vitro (Kjeken *et al*., 2004). In MLN64-depleted cells, however, the cargo bearing dispersed endosomes were situated between the peripheral actin cables, and endosome-associated actin labeling was seldom observed. In contrast, WT MLN64 overexpression increased the number of actin patches in MLN64-positive late endosomes, whereas ΔSTART had no significant effect (Figure 8, A and B). A similar phenotype of increased phalloidin labeling was observed in MLN64-overexpressing endosomes in COS cells (our unpublished data). Arp2/3 complex plays a key role in the regulation of actin polymerization and localizes to sites of dynamic actin (Machesky and Gould, 1999). We therefore analyzed the subcellular localization of p34-Arc, a subunit of the Arp2/3 complex, in MLN64-depleted or -overexpressing cells. As shown previously, anti-p34-Arc immunostaining was visualized in lamellipodia as well as in cytoplasmic punctate structures (Welch *et al*., 1997) (Figure 9A). Analogously to phalloidin staining, the overall staining pattern of p34-Arc was not perturbed upon altering MLN64 levels (our unpublished data). However, when individual MLN64-overexpressing endosomes were analyzed, we found that WT MLN64 but not ΔSTART significantly increased the number of organelles decorated with p34-Arc immunoreactivity (Figure 9B). Conversely, MLN64 depletion resulted in a moderate but significant decrease in p34-Arc labeling of late endocytic organelles.

To analyze the association of late endocytic organelles with actin cytoskeleton in vitro, we studied the amount of Lamp2 cosedimenting with actin under conditions when microtubules were depolymerized. The nocodazole treatment and a short centrifugation time (5 min) were used to promote conditions that favor pelleting of membranes in association with the actin cytoskeleton. Under these conditions, a minor fraction of actin and Lamp2 was recovered in the pellet both in control and MLN64-depleted cells. In contrast, β-tubulin was hardly detectable (Figure 10A). Addition of cytochalasin D to the PNS did not abolish the sedimentation of actin or Lamp2 (our unpublished data). However, the fraction of Lamp2 pelleted relative to ac-

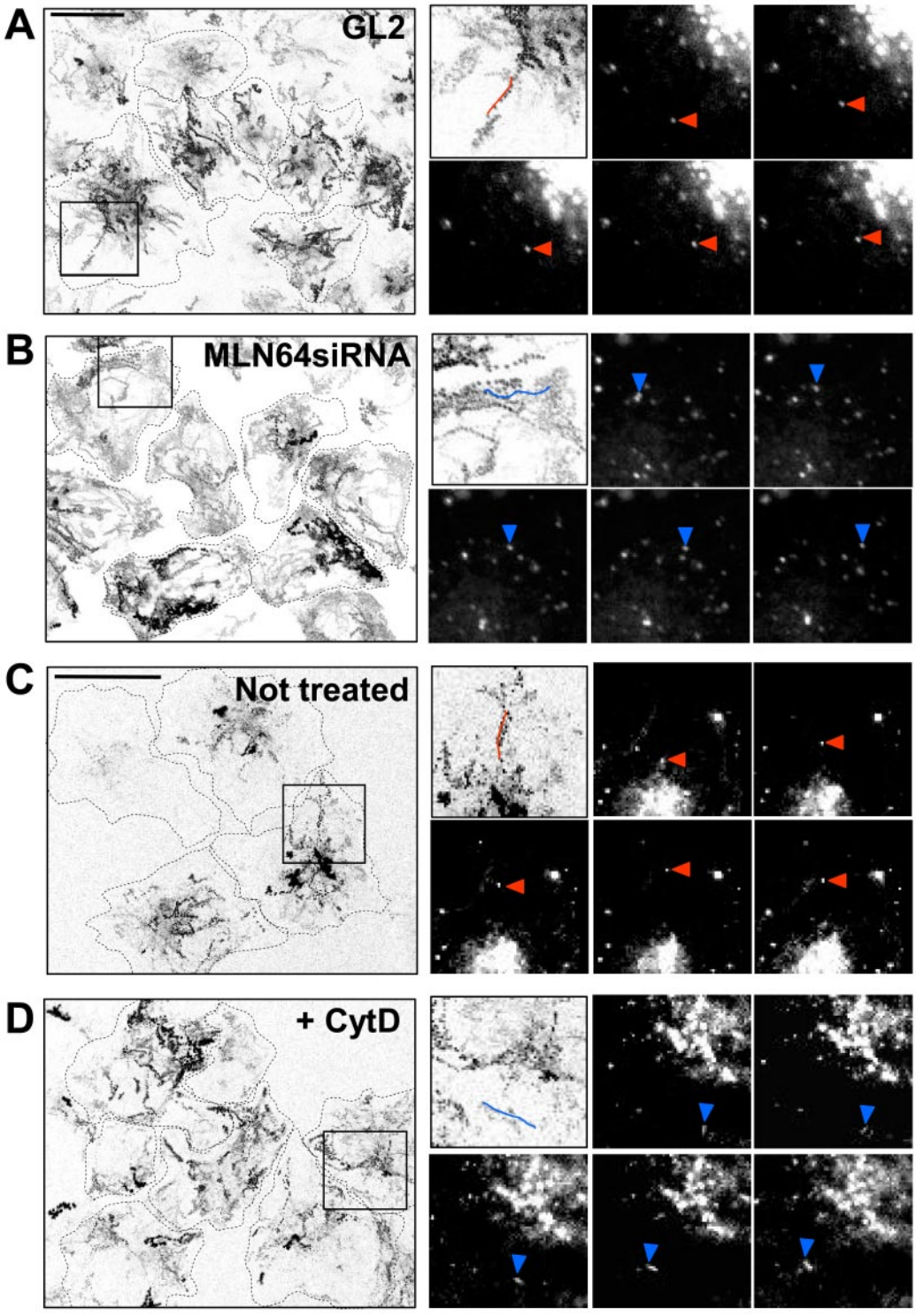

Figure 6. MLN64 depletion and actin disruption have similar effects on endosome motility in HeLa cells. Control (GL2) (A) or MLN64-depleted cells (MLN64siRNA) (B) were labeled with DiI-LDL and then imaged for 4 min (1 image/s). In C and D, untransfected cells were labeled with DiI-LDL and further incubated for 2.5 h, the last 1 h with or without 0.2 μM cytochalasin D, and imaged as described in A and B. The trajectories of labeled endosomes from a field of cells are shown (left). Cell boundaries are sketched with dotted lines. Boxed areas are depicted in the top left insets. Video frames at 2-s intervals are shown, and the individual endosomes producing the tracks outlined in the top left insets are indicated with arrowheads. Examples of stellate trajectories are highlighted in red and peripheral trajectories in blue. Bars, 20 μm.

tin was clearly reduced compared with control without cytochalasin D (Figure 10B). Similarly to actin disruption, MLN64 knockdown decreased the fraction of Lamp2 cosedimenting with actin (Figure 10, A and B). These data suggest that Lamp2-positive organelles displayed reduced association with actin when MLN64 was depleted.

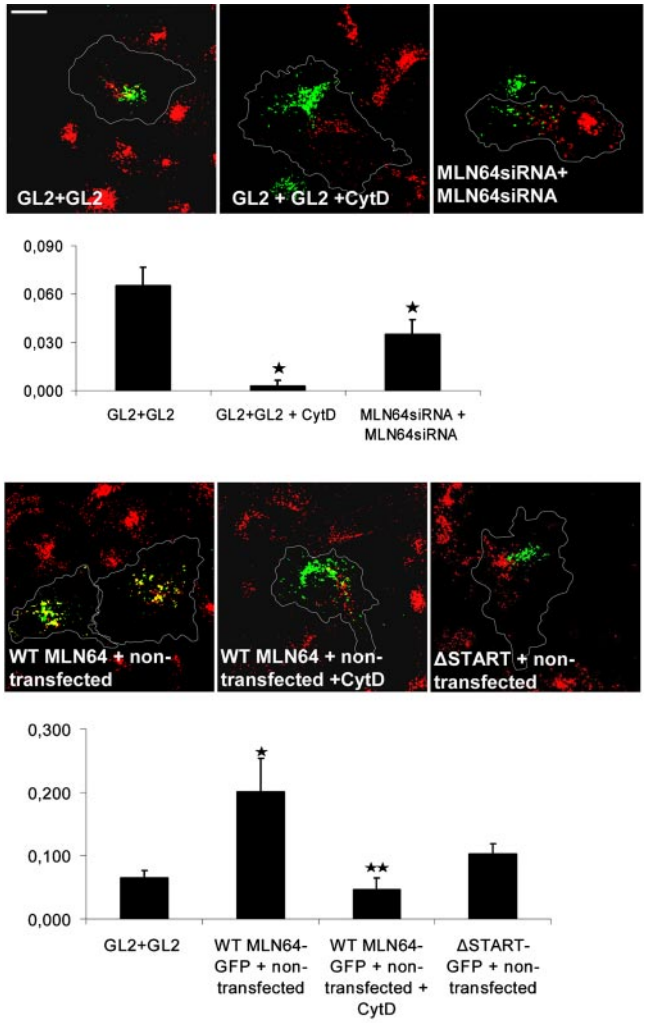

Figure 7. Effect of MLN64 depletion or overexpression in the fusion of late endocytic organelles in HeLa cells. Nontransfected and GL2 control or MLN64siRNA-transfected cells were labeled with fluorescein or rhodamine-conjugated dextrans. Alternatively, cells were transfected with GFP-fused WT MLN64 or ΔSTART. The cells were then cocultured as indicated, fused with PEG, and incubated for 1 h either in normal growth medium or medium supplemented with 0.2 μM cytochalasin D. The degree of overlay was determined by Pearson's correlation coefficient. The values are from 23 to 55 individual cells, *$p < 0.05$ between GL2 control and GL2 + cytochalasin D, MLN64siRNA, or WT MLN64-GFP overexpression, **$p < 0.05$ between WT MLN64-GFP overexpression and WT MLN64-GFP overexpression + cytochalasin D. Images are confocal and represent a single focal plane. Bar, 20 μm.

DISCUSSION

MLN64 is a cholesterol-binding protein whose physiological role is not understood. It has been suggested to function in the export of late endosomal cholesterol to other cellular acceptors, such as mitochondria, perhaps acting as a downstream effector of the NPC1 and NPC2 proteins (Strauss *et al*., 2002; Zhang *et al*., 2002). However, in a recent study describing a mouse with mutated START domain of MLN64, no obvious sterol-related phenotype was observed (Kishida *et al*., 2004). Consistently with this study, the findings presented here did not reveal an indispensable role for MLN64 in late endosomal cholesterol export. Overexpression of MLN64 did not reduce cholesterol accumulation in NPC1-deficient cells but instead was able to promote late endosomal sterol deposition in COS cells. Moreover, MLN64 depletion did not result in an NPC-like cholesterol accumulation in late endocytic organelles nor did it impair cellular cholesterol homeostasis as measured by cholesterol esterification or efflux. Although these findings do not exclude the possibility that MLN64 transfers sterol from late endocytic organelles to other cellular sites, the most obvious effects of MLN64 depletion were found on endosome dynamics instead of cellular sterol balance.

Endosomes are thought to contain a mosaic of structural and functional domains (Gruenberg, 2001). For example, specific membrane domains defined by distinct Rab proteins have been visualized in early and late endosomes (Sönnichsen *et al*., 2000; Barbero *et al*., 2002). Similarly, MLN64 seems to reside in distinct membrane domains of late endosomes (Alpy *et al*., 2001; this study). In cells depleted of MLN64, the movement of endocytic cargo containing late endosomes was altered, leading to their dispersal to the cell periphery. The peripheral endosomes were motile and moved along microtubules. Importantly, the dispersion phenotype could not be complemented by MLN64 mutants deficient in sterol binding. This suggests that MLN64-mediated changes in sterol distribution of late endosome membranes contribute to their correct positioning, perhaps by affecting the association of endosomes with cytoskeletal elements. Although cholesterol is normally not enriched in late endocytic organelles (Hölttä-Vuori *et al*., 2002; Kobayashi *et al*., 2002; Möbius *et al*., 2003), it has a substantial effect on their dynamics (Ko *et al*., 2001; Zhang *et al*., 2001; Lebrand *et al*., 2002). It has been shown that abnormal cholesterol loading influences the association of late endosomes to microtubules via the Rab7 cycle (Lebrand *et al*., 2002). However, we did not observe impaired recruitment of the Rab7–RILP–dynein machinery in MLN64-depleted cells, nor were we able to rescue the endosome dispersion with overexpression of RILP. These results suggest that the molecular mechanism underlying the organelle dispersion in MLN64-depleted cells is distinct from the Rab7–dynein machinery.

The actin cytoskeleton has been implicated in the dynamics of late endosomes and lysosomes. Disrupting filamentous actin results in the redistribution of late endocytic organelles to the cell periphery, altered endosome motility and inhibition of cargo degradation (van Deurs *et al*., 1995; Durrbach *et al*., 1996; Cordonnier *et al*., 2001). The involvement of actin in endosome/lysosome motility may improve the probability of organelle fusion and content mixing required for lysosomal proteolysis (van Deurs *et al*., 1995). Indeed, actin has been shown to be involved in the fusion between mature endosomes and lysosomes in mammalian cells (van Deurs *et al*., 1995), between isolated late endosomes (Kjeken *et al*., 2004) and in vacuole fusion in yeast (Eitzen *et al*., 2002). However, the molecular mechanisms governing the binding of actin to late endosomes remain poorly understood.

Several lines of evidence suggest that MLN64 modulates the interaction of late endosomes with actin. First, the effects of MLN64 depletion on late endosomal dynamics were strikingly similar to those of actin disruption, i.e., scattering of late endocytic organelles, attenuated cargo degradation, and impaired clustering and/or fusion of late endocytic organelles. Conversely, overexpression of MLN64 enhanced fusion in an actin-dependent manner. Second, endosomal MLN64 levels correlated with the association of actin with late endosomes. MLN64 overexpression resulted in the increased formation of actin patches on the organelles harboring the protein, whereas upon MLN64 depletion, late endo-

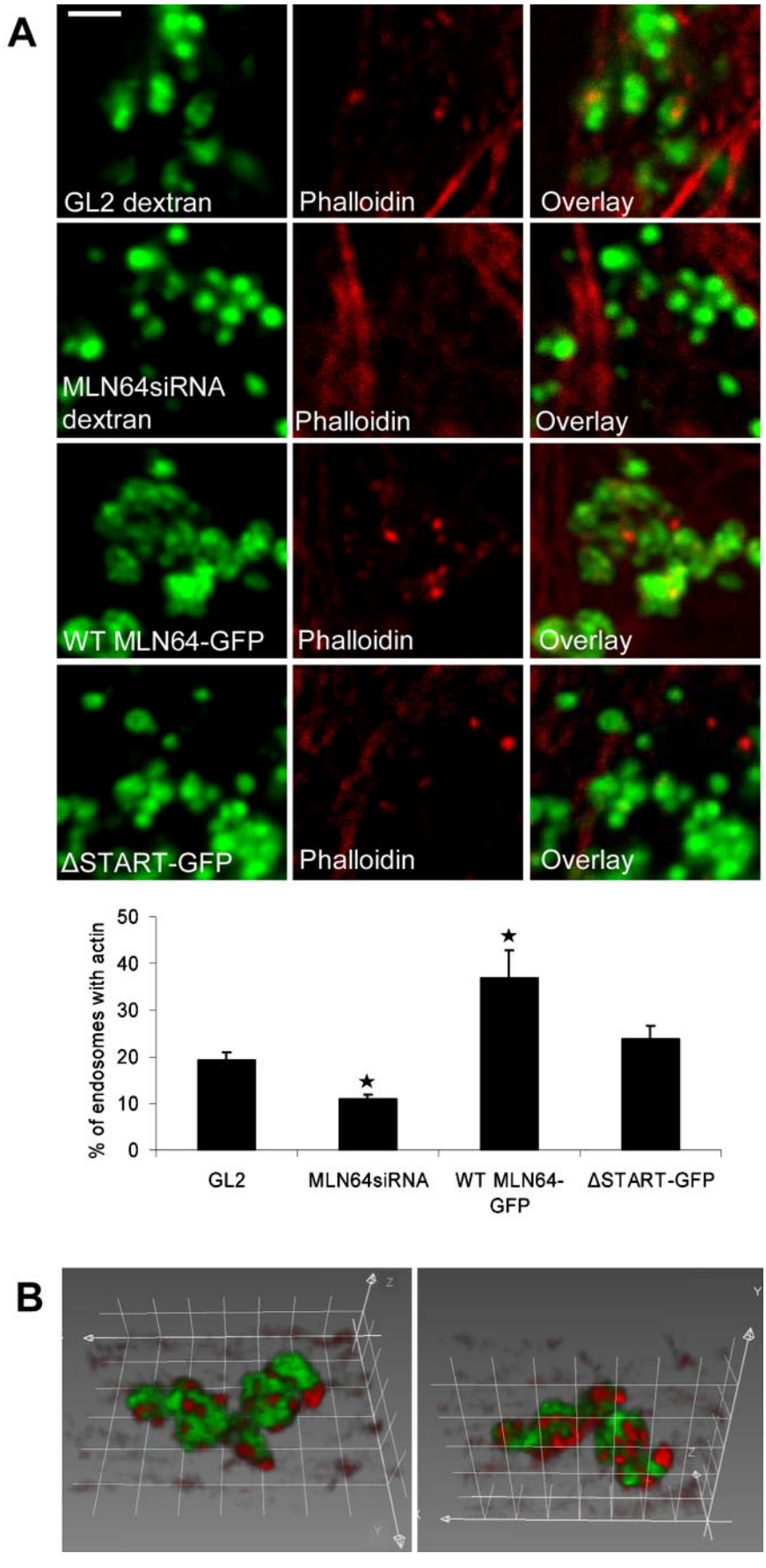

Figure 8. MLN64 modulates the association of actin with late endosomes in HeLa cells. (A) Phalloidin staining of GL2 control and MLN64siRNA-transfected cells labeled with fluorescein-conjugated dextran and HeLa cells transfected with GFP-fused WT MLN64 or ΔSTART. The percentage of late endocytic organelles decorated with actin patches was analyzed from confocal sections of four to 10 individual cells at high magnification, n of endosomes ≥358 per treatment, *$p < 0.05$ between GL2 control and MLN64siRNA or WT MLN64-GFP overexpression. Images are confocal and represent a single focal plane. Bars, 2 μm. (B) Three-dimensional rendering of WT MLN64-GFP–positive endosomes stained with phalloidin is shown from two angles. Grid spacing, 1 μm.

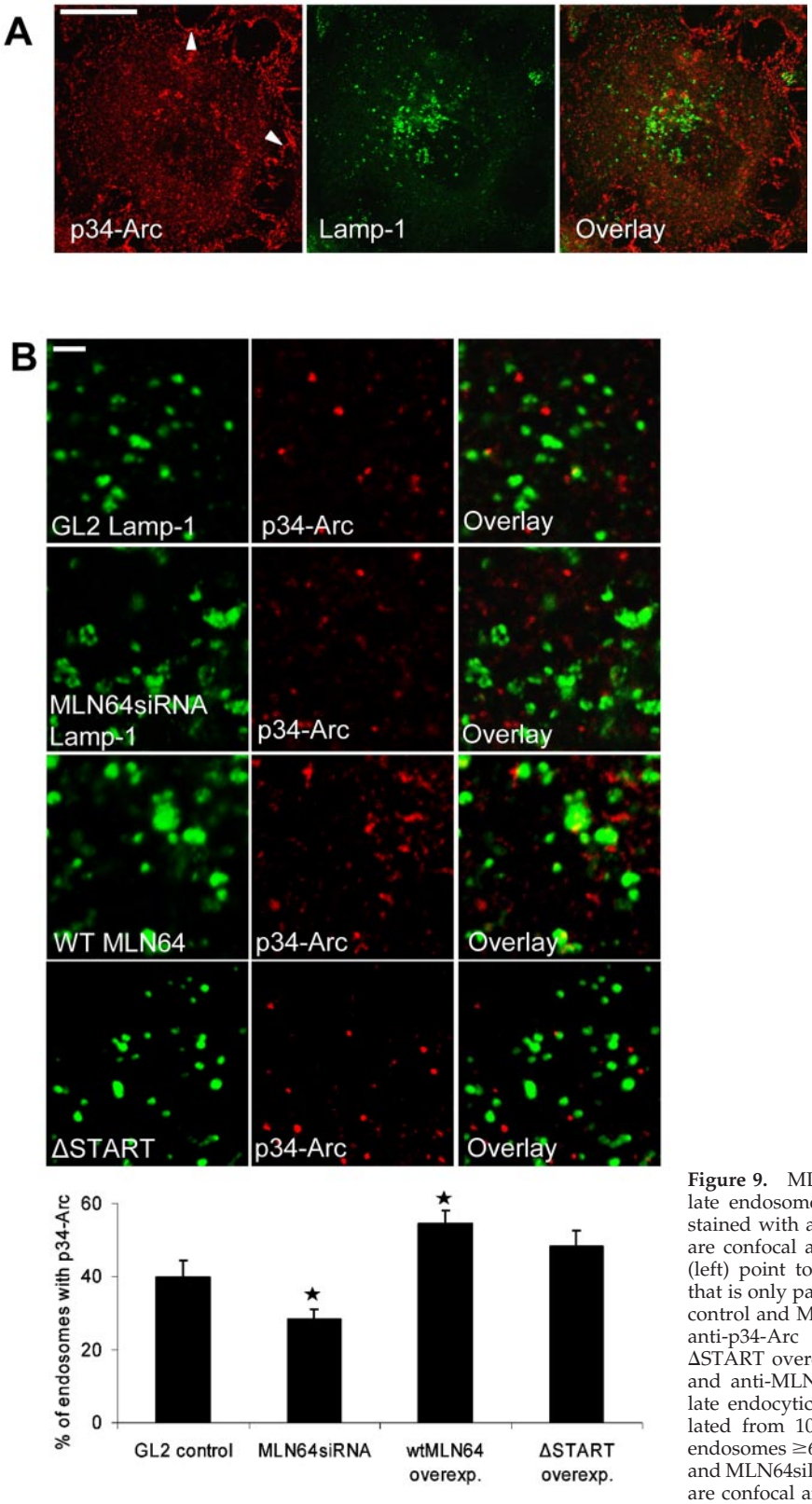

Figure 9. MLN64 modulates the association of p34-Arc with late endosomes in HeLa cells. (A) Control HeLa cells were stained with anti-p34-Arc and anti-Lamp1 antibodies. Images are confocal and represent a single focal plane. Arrowheads (left) point to the prominent lamellipodial p34-Arc staining that is only partially visible in the section. Bar, 20 μm. (B) GL2 control and MLN64siRNA transfected cells were stained with anti-p34-Arc and anti-Lamp1 antibodies. WT MLN64 or ΔSTART overexpressing cells were stained with anti-p34-Arc and anti-MLN64 (N-terminal) antibodies. The percentage of late endocytic organelles decorated with p34-Arc was calculated from 10 to 12 individual cells as in Figure 8A, n of endosomes $\geq$624 per treatment, *$p < 0.05$ between GL2 control and MLN64siRNA or WT MLN64-GFP overexpression. Images are confocal and represent a single focal plane. Bars, 2 μm.

cytic structures had fewer actin patches. Third, the Arp2/3 complex subunit p34-Arc showed a similar tendency, being increasingly associated with late endocytic organelles upon MLN64 overexpression and exhibiting diminished association upon decrease of MLN64 levels. This finding suggests that MLN64 is part of the machinery governing actin nucleation from late endosomes. Fourth, when MLN64 was depleted late endocytic organelles displayed reduced asso-

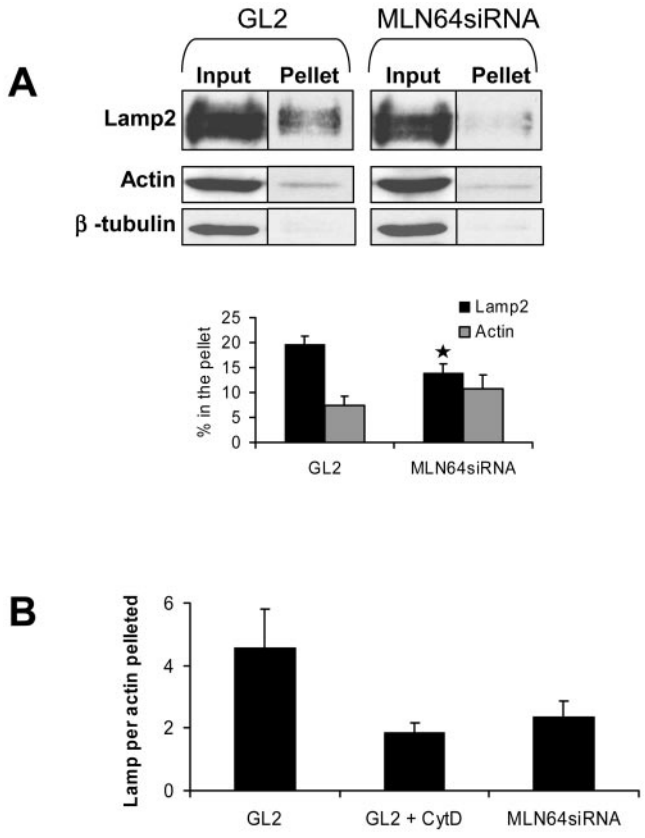

Figure 10. MLN64 depletion decreases the sedimentation of Lamp2-positive organelles with actin. (A) PNS from control (GL2) or MLN64-depleted cells (MLN64siRNA) was incubated in the presence of 100 μM nocodazole and pelleted at 100,000 $\times$ *g* for 5 min. Aliquots of PNS before centrifugation (input) and pellets were immunoblotted using anti-Lamp2, anti-actin, and anti-β-tubulin antibodies. The amount of Lamp2 and actin pelleted was determined by densitometric scanning and expressed as percentage of input (mean of 12 samples). *$p < 0.05$ between GL2 and MLN64siRNA. (B) The fraction of Lamp2 sedimented was normalized with the fraction of actin pelleted. GL2 + CytD indicates PNS of control (GL2) cells incubated in the presence of 4 μM cytochalasin D. Bars represent mean of seven to 12 samples.

ciation with actin, as suggested by the decreased cosedimentation of Lamp2-positive membranes with actin. Finally, actin-dependent late endosome dynamics seemed to be functionally connected to MLN64-mediated sterol transfer as MLN64 mutants defective in cholesterol binding and endosomal sterol loading were not able to rescue endosome dispersion in MLN64-depleted cells.

Interestingly, the transmembrane region of MLN64 (ΔSTART) is capable of interacting with cholesterol, perhaps to retain cholesterol on its way to the cytoplasmic START domain (Alpy *et al*., 2005). We found that the ΔSTART mutant also promoted sterol accumulation in late endosomes, albeit less effectively than the WT protein. Previously, overexpression of ΔSTART MLN64 was reported to result in an NPC-like cholesterol accumulation phenotype (Zhang *et al*., 2002). These effects may be explained by the residual sterol affinity of ΔSTART, which might act in cooperation with the WT protein present in the cells. However, ΔSTART was not sufficient to restore the endosome dispersion or increase endosome actin recruitment, suggesting that the function of the cholesterol-binding START domain is needed to support actin-dependent late endosome dynamics.

There is no evidence to suggest that the connection between MLN64 and actin is direct. Rather, we envisage that MLN64-induced changes in the sterol distribution of the endosome membrane may promote the recruitment of components of the actin nucleation machinery. The precise mechanism of actin recruitment remains to be elucidated but may involve, for example, phosphoinositides that are known regulators of actin dynamics and sensitive to the cholesterol content in the membrane (Kwik *et al*., 2003). Interestingly, recent data indicate that sterol enrichment of yeast vacuolar membranes promotes actin remodeling and enhances vacuole membrane fusion (Tedrick *et al*., 2004). We propose that MLN64-mediated local sterol enrichment of late endosomal membranes facilitates the association of late endosomes with the actin cytoskeleton, thereby governing their motility, degradative activity, and fusion. As such, MLN64 would set precedence for linking the sterol organization and actin-mediated dynamics of late endocytic organelles in mammalian cells.

ACKNOWLEDGMENTS

We thank F. Maxfield and S. Mukherjee for help with DHE labeling; J. Hurley and Y. Tsujishita for pET 22b-MLN64-START construct and helpful discussions; C. Thiele for [^{3}H]photocholesterol; C. Bucci for RILP-construct and antibody; K. Hirschberg for fibroblast poration protocol; C. Tomasetto, P. Lappalainen, and E. Coudrier for helpful discussions; and D. Hentsch, I. Stoll, M. Oulad-Abdelghani, and P. Eberling for technical assistance. This study was supported by the Academy of Finland, Ara Parseghian Medical Research Foundation, Helsinki Biomedical Graduate School, Sigrid Juselius Foundation, and Finnish Cultural Foundation.

REFERENCES

Alpy, F., Stoeckel, M. E., Dierich, A., Escola, J. M., Wendling, C., Chenard, M. P., Vanier, M. T., Gruenberg, J., Tomasetto, C., and Rio, M. C. (2001). The steroidogenic acute regulatory protein homolog MLN64, a late endosomal cholesterol-binding protein. J. Biol. Chem. *276*, 4261–4269.

Alpy, F., Latchumanan, V. K., Kedinger, V., Janoshazi, A., Thiele, C., Wendling, C., Rio, M. C., and Tomasetto, C. (2005). Functional characterization of the MENTAL domain. J. Biol. Chem. *280*, 17945–17952.

Alpy, F., Wendling, C., Rio, M. C., and Tomasetto, C. (2002). MENTHO, a MLN64 homologue devoid of the START domain. J. Biol. Chem. *277*, 50780–50787.

Arai, R., Geffard, M., and Calas, A. (1992). Intensification of labelings of the immunogold silver staining method by gold toning. Brain Res. Bull. *28*, 343–345.

Barbero, P., Bittova, L., and Pfeffer, S. R. (2002). Visualization of Rab9-mediated vesicle transport from endosomes to the trans-Golgi in living cells. J. Cell Biol. *156*, 511–518.

Blom, W. M., de Bont, H. J., and Nagelkerke, J. F. (2003). Regional loss of the mitochondrial membrane potential in the hepatocyte is rapidly followed by externalization of phosphatidylserines at that specific site during apoptosis. J. Biol. Chem. *278*, 12467–12474.

Cantalupo, G., Alifano, P., Roberti, V., Bruni, C. B., and Bucci, C. (2001). Rab-interacting lysosomal protein (RILP): the Rab7 effector required for transport to lysosomes. EMBO J. *20*, 683–693.

Cordonnier, M. N., Dauzonne, D., Louvard, D., and Coudrier, E. (2001). Actin filaments and myosin I alpha cooperate with microtubules for the movement of lysosomes. Mol. Biol. Cell *12*, 4013–4029.

Durrbach, A., Louvard, D., and Coudrier, E. (1996). Actin filaments facilitate two steps of endocytosis. J. Cell Sci. *109*, 457–465.

Eitzen, G., Wang, L., Thorngren, N., and Wickner, W. (2002). Remodeling of organelle-bound actin is required for yeast vacuole fusion. J. Cell Biol. *158*, 669–679.

Elbashir, S. M., Harborth, J., Lendeckel, W., Yalcin, A., Weber, K., and Tuschl, T. (2001). Duplexes of 21-nucleotide RNAs mediate RNA interference in cultured mammalian cells. Nature *411*, 494–498.

Gruenberg, J. (2001). The endocytic pathway: a mosaic of domains. Nat. Rev. Mol. Cell. Biol. *2*, 721–730.

Hao, M., Lin, S. X., Karylowski, O. J., Wustner, D., McGraw, T. E., and Maxfield, F. R. (2002). Vesicular and non-vesicular sterol transport in living cells. The endocytic recycling compartment is a major sterol storage organelle. J. Biol. Chem. *277*, 609–617.

Hölttä-Vuori, M., Määttä, J., Ullrich, O., Kuismanen, E., and Ikonen, E. (2000). Mobilization of late-endosomal cholesterol is inhibited by Rab guanine nucleotide dissociation inhibitor. Curr. Biol. *10*, 95–98.

Hölttä-Vuori, M., Tanhuanpää, K., Möbius, W., Somerharju, P., and Ikonen, E. (2002). Modulation of cellular cholesterol transport and homeostasis by Rab11. Mol. Biol. Cell *13*, 3107–3122.

Ikonen, E., and Hölttä-Vuori, M. (2004). Cellular pathology of Niemann-Pick type C disease. Semin. Cell Dev. Biol. *15*, 445–454.

Jordens, I., Fernandez-Borja, M., Marsman, M., Dusseljee, S., Janssen, L., Calafat, J., Janssen, H., Wubbolts, R., and Neefjes, J. (2001). The Rab7 effector protein RILP controls lysosomal transport by inducing the recruitment of dynein-dynactin motors. Curr. Biol. *11*, 1680–1685.

Kishida, T., Kostetskii, I., Zhang, Z., Martinez, F., Liu, P., Walkley, S. U., Dwyer, N. K., Blanchette-Mackie, E. J., Radice, G. L., and Strauss, J. F., 3rd. (2004). Targeted mutation of the MLN64 START domain causes only modest alterations in cellular sterol metabolism. J. Biol. Chem. *279*, 19276–19285.

Kjeken, R., *et al*. (2004). Fusion between phagosomes, early and late endosomes: a role for actin in fusion between late, but not early endocytic organelles. Mol. Biol. Cell *15*, 345–358.

Ko, D. C., Gordon, M. D., Jin, J. Y., and Scott, M. P. (2001). Dynamic movements of organelles containing Niemann-Pick C1 protein: NPC1 involvement in late endocytic events. Mol. Biol. Cell *12*, 601–614.

Kobayashi, T., Beuchat, M. H., Chevallier, J., Makino, A., Mayran, N., Escola, J. M., Lebrand, C., Cosson, P., Kobayashi, T., and Gruenberg, J. (2002). Separation and characterization of late endosomal membrane domains. J. Biol. Chem. *277*, 32157–32164.

Kwik, J., Boyle, S., Fooksman, D., Margolis, L., Sheetz, M. P., and Edidin, M. (2003). Membrane cholesterol, lateral mobility, and the phosphatidylinositol 4,5-bisphosphate-dependent organization of cell actin. Proc. Natl. Acad. Sci. USA *100*, 13964–13969.

Lebrand, C., Corti, M., Goodson, H., Cosson, P., Cavalli, V., Mayran, N., Faure, J., and Gruenberg, J. (2002). Late endosome motility depends on lipids via the small GTPase Rab7. EMBO J. *21*, 1289–1300.

Machesky, L. M., and Gould, K. L. (1999). The Arp2/3 complex: a multifunctional actin organizer. Curr. Opin. Cell Biol. *11*, 117–121.

Möbius, W., Van Donselaar, E., Ohno-Iwashita, Y., Shimada, Y., Heijnen, H. F., Slot, J. W., and Geuze, H. J. (2003). Recycling compartments and the internal vesicles of multivesicular bodies harbor most of the cholesterol found in the endocytic pathway. Traffic *4*, 222–231.

Moog-Lutz, C., Tomasetto, C., Regnier, C. H., Wendling, C., Lutz, Y., Muller, D., Chenard, M. P., Basset, P., and Rio, M. C. (1997). MLN64 exhibits homology with the steroidogenic acute regulatory protein (STAR) and is overexpressed in human breast carcinomas. Int. J. Cancer *71*, 183–191.

Mukherjee, S., Zha, X., Tabas, I., and Maxfield, F. R. (1998). Cholesterol distribution in living cells: fluorescence imaging using dehydroergosterol as a fluorescent cholesterol analog. Biophys. J. *75*, 1915–1925.

Raiborg, C., Bache, K. G., Mehlum, A., Stang, E., and Stenmark, H. (2001). Hrs recruits clathrin to early endosomes. EMBO J. *20*, 5008–5021.

Richardson, S. C., Winistorfer, S. C., Poupon, V., Luzio, J. P., and Piper, R. C. (2004). Mammalian late vacuole protein sorting orthologues participate in early endosomal fusion and interact with the cytoskeleton. Mol. Biol. Cell *15*, 1197–1210.

Seemann, J., Jokitalo, E. J., and Warren, G. (2000). The role of the tethering proteins p115 and GM130 in transport through the Golgi apparatus in vivo. Mol. Biol. Cell *11*, 635–645.

Sonnichsen, B., de Renzis, S., Nielsen, E., Rietdorf, J., and Zerial, M. (2000). Distinct membrane domains on endosomes in the recycling pathway visualized by multicolor imaging of Rab4, Rab5, and Rab11. J. Cell Biol. *149*, 901–914.

Strauss, J. F., 3rd, Liu, P., Christenson, L. K., and Watari, H. (2002). Sterols and intracellular vesicular trafficking: lessons from the study of NPC1. Steroids *67*, 947–951.

Tedrick, K., Trischuk, T., Lehner, R., and Eitzen, G. (2004). Enhanced membrane fusion in sterol-enriched vacuoles bypasses the Vrp1p requirement. Mol. Biol. Cell *15*, 4609–4621.

Thiele, C., Hannah, M. J., Fahrenholz, F., and Huttner, W. B. (2000). Cholesterol binds to synaptophysin and is required for biogenesis of synaptic vesicles. Nat. Cell Biol. *2*, 42–49.

Tsujishita, Y., and Hurley, J. H. (2000). Structure and lipid transport mechanism of a StAR-related domain. Nat. Struct. Biol. *7*, 408–414.

van Deurs, B., Holm, P. K., Kayser, L., and Sandvig, K. (1995). Delivery to lysosomes in the human carcinoma cell line HEp-2 involves an actin filament-facilitated fusion between mature endosomes and preexisting lysosomes. Eur. J. Cell Biol. *66*, 309–323.

Vitelli, R., Santillo, M., Lattero, D., Chiariello, M., Bifulco, M., Bruni, C. B., and Bucci, C. (1997). Role of the small GTPase Rab7 in the late endocytic pathway. J. Biol. Chem. *272*, 4391–4397.

Watari, H., Arakane, F., Moog-Lutz, C., Kallen, C. B., Tomasetto, C., Gerton, G. L., Rio, M. C., Baker, M. E., and Strauss, J. F., 3rd. (1997). MLN64 contains a domain with homology to the steroidogenic acute regulatory protein (StAR) that stimulates steroidogenesis. Proc. Natl. Acad. Sci. USA *94*, 8462–8467.

Welch, M. D., DePace, A. H., Verma, S., Iwamatsu, A., and Mitchison, T. J. (1997). The human Arp2/3 complex is composed of evolutionarily conserved subunits and is localized to cellular regions of dynamic actin filament assembly. J. Cell Biol. *138*, 375–384.

Westerman, J., Wirtz, K. W., Berkhout, T., van Deenen, L. L., Radhakrishnan, R., and Khorana, H. G. (1983). Identification of the lipid-binding site of phosphatidylcholine-transfer protein with phosphatidylcholine analogs containing photoactivable carbene precursors. Eur. J. Biochem. *132*, 441–449.

Zhang, M., Dwyer, N. K., Love, D. C., Cooney, A., Comly, M., Neufeld, E., Pentchev, P. G., Blanchette-Mackie, E. J., and Hanover, J. A. (2001). Cessation of rapid late endosomal tubulovesicular trafficking in Niemann-Pick type C1 disease. Proc. Natl. Acad. Sci. USA *98*, 4466–4471.

Zhang, M., Liu, P., Dwyer, N. K., Christenson, L. K., Fujimoto, T., Martinez, F., Comly, M., Hanover, J. A., Blanchette-Mackie, E. J., and Strauss, J. F., 3rd. (2002). MLN64 mediates mobilization of lysosomal cholesterol to steroidogenic mitochondria. J. Biol. Chem. *277*, 33300–33310.